Model assessment for direct contact condensation induced by a sub-cooled water jet in a circular pipe

Riccardo Cocci, Alberto Ghione, Lucia Sargentini, Guillaume Damblin, Didier D Lucor

MODEL ASSESSMENT FOR DIRECT CONTACT CONDENSATION INDUCED BY A SUB-COOLED WATER JET IN A CIRCULAR PIPE

Riccardo Cocci[a1], Alberto Ghione[a], Lucia Sargentini[a], Guillaume Damblin[a], Didier Lucor[b]

[a]Université Paris-Saclay, CEA, Service de Thermohydraulique et de Mécanique des Fluides 91191, Gif-sur-Yvette, France

[b]Laboratoire Interdisciplinaire des Sciences du Numérique LISN-CNRS, F-91403, Orsay, France

ABSTRACT

In this paper, the condensation induced by a sub-cooled water injection in a circular horizontal pipe with a two-phase stratified flow is investigated. The focus of the work is to review the physical models or correlations predicting the condensation heat transfer coefficient and assess them against an experimental database.

Three experiments, namely COSI, TOPFLOW-PTS and UPTF, are consolidated in a substantial database. They have different configurations and complexity, covering a wide range of injection mass flowrate, temperature and pressure. A thermal-hydraulic analysis is performed, resulting in reliable and coherent experimental data.

The condensation models found in the literature are based on the modelling of the Nusselt number through several dimensionless numbers. The assessment of these correlations against the experimental database provides poor results. Thus, a new approach is proposed.

The cold jet is modelled as a heat exchanger, which is described by a condensation potential. The analytical formula of the potential is found starting from an energy balance at the injection, showing that the condensation depends on the jet geometrical shape and a parameter η.

A new correlation for the parameter η is calibrated against the COSI and TOPFLOW-PTS experiments, significantly reducing the average standard deviation between evaluations and experimental data. The new correlation is then applied to an independent database, i.e. the UPTF experiments. The results show good agreement between the calculated and

[1] Corresponding author
E-mail addresses: riccardo.cocci@cea.fr, alberto.ghione@cea.fr, lucia.sargentini@cea.fr, guillaume.damblin@cea.fr, didier.lucor@lisn.upsaclay.fr

experimental values, proving the capability of the new model to accurately predict the condensation at the injection.

Keywords: Direct Contact Condensation, Liquid jet, Physical model assessment, Stratified flow

Nomenclature

A	area $[m^2]$
c_p	specific heat capacity at constant pressure $\left[{}^{J}/_{kg \cdot K}\right]$
d	diameter $[m]$
D	test section diameter $[m]$
Fr	Froude number $\sqrt{\frac{u^2}{g \cdot l_{Fr}}}$
$\dot{G}$	specific mass flowrate $\left[{}^{kg}/_{s \cdot m^2}\right]$
g	gravity constant $\left[{}^{m}/_{s^2}\right]$
h	heat transfer coefficient $\left[{}^{W}/_{m^2 \cdot K}\right]$
H	liquid height in the test section $[m]$
i	specific enthalpy $\left[{}^{J}/_{kg}\right]$
i_{lg}	latent heat of condensation $\left[{}^{J}/_{kg}\right]$
k	thermal conductivity $\left[{}^{W}/_{m \cdot K}\right]$
l	characteristic length $[m]$
L	jet length $[m]$

$\dot{m}$	mass flowrate $\left[{kg}/{s}\right]$
Nu	Nusselt number $\frac{h \cdot l_{Nu}}{k}$
Pr	Prandtl number $\frac{\mu \cdot c_p}{k}$
$\dot{Q}$	volumetric flowrate $\left[{m^3}/{s}\right]$
$\dot{q}$	heat flux $[W]$
$\dot{q}$"	specific heat flux $\left[{W}/{m^2}\right]$
Re	Reynolds number $\frac{\rho \cdot u \cdot l_{Re}}{\mu}$
St	Stanton number ${Nu}/{(Re \cdot Pr)}$
T	temperature $[K]$
u	velocity $[{m}/{s}]$

Greek symbols

α	void fraction
μ	dynamic viscosity $[Pa \cdot s]$
ρ	density $\left[{kg}/{m^3}\right]$
σ	standard deviation

Subscripts

cond	condensation
ex	exchange

g	gas
inj	injection
l	liquid
pot	potential
ps	pump simulator
ref	calculated at the reference temperature
sat	saturation

1. Introduction

Direct Contact Condensation (DCC) phenomena between steam and sub-cooled water are of great importance in various industrial fields such as nuclear [1], chemical [2] and manufacturing [3].

In the literature, two main configurations for the occurrence of DCC have been widely investigated: the injection of steam in large liquid pools (e.g. [4], [5], [6], [7], [8]) and the injection of sub-cooled water in large volumes of steam (e.g. [9], [10], [11]). On the contrary, the DCC induced by a sub-cooled water injection in a circular horizontal pipe with a two-phase stratified flow was studied in a limited number of articles. In Fig. 1, the phenomenon is briefly illustrated. There, the cold water (in light blue) flows mainly from the left to the right of the pipe. The gas phase (in yellow) consists of pure steam without non-condensable gases that can flow in either a co-current or counter-current way.

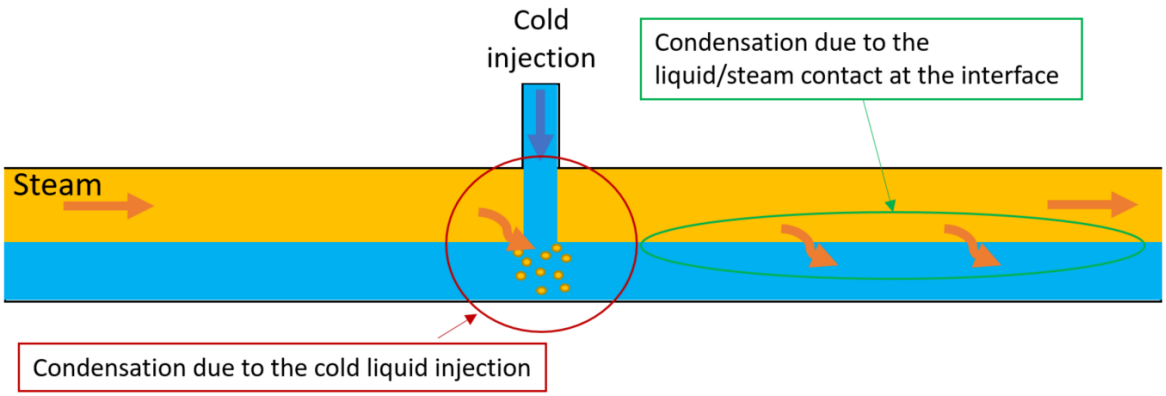

Fig. 1 *Main phenomena occurring at a sub-cooled injection into a two-phase flow.*

Two main condensation zones are identified: the jet and the stratified condensation. The former is due to the contact of the cylindrical jet with the steam and then its impact in the liquid flow, the latter to the contact of the steam and the liquid at the interface in the stratified flow far away from the jet. In this article, we are interested on studying and modelling the condensation at the injection in the framework of system codes development.

In Fig. 2, the main local DCC phenomena in the injection region are represented [12]. The cold water is injected in the pipe, plunging in a two-phase flow of hot water (in dark blue) and pure steam.

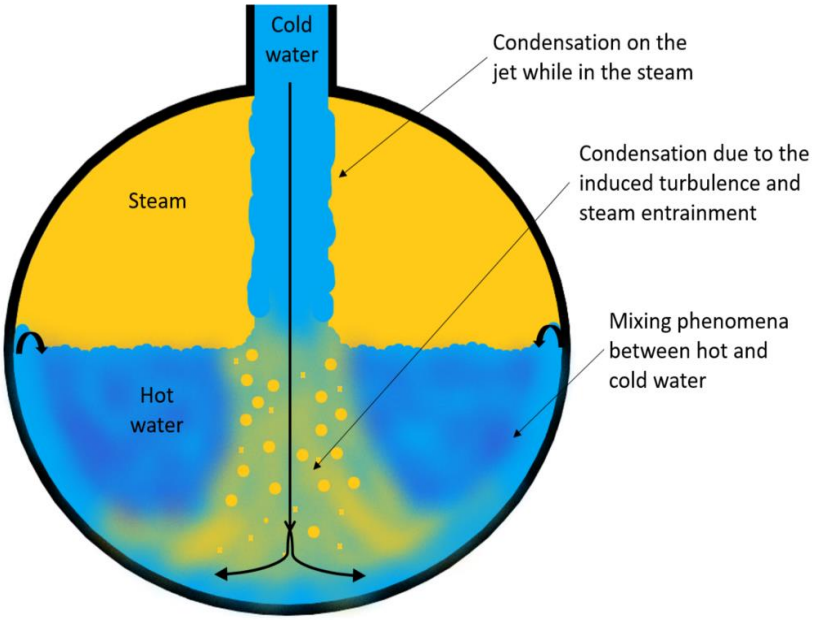

Fig. 2 *Main local DCC phenomena occurring at the injection.*

Different local condensation phenomena are identified. Before the impact with the hot water, the steam condensates over the rough cold jet surface. After the impact, the condensation is

mostly driven by the steam entrainment in the liquid phase [13] and the induced turbulence enhances the heat exchange mechanism. In the liquid phase, mixing phenomena take place between the cold water rebounding the walls and the hot water [14]. Moreover, the injection itself and the lateral rebounds create a wavy liquid-steam surface, enhancing the steam condensation [15].

In 1989, Bestion and Gros d'Aillon [16] described the DCC phenomenology induced by a water jet in a circular horizontal pipe based on the experimental results obtained in the facility COSI (COndensation at Safety Injection). They found out that the biggest contribution to the global condensation in the test section was associated to the jet impact into the two-phase stratified flow and supposed that the main DCC mechanism was due to turbulence generated by impact of the water jet into the stratified water. To predict the steam condensation in the injection zone, they developed a correlation based on three experimental series of the COSI experiments carried out with the Framatome configuration of the test section (see description of the test facility in Section 2.1). The dimensionless numbers, Nusselt, Reynolds and Prandtl, were employed.

An improvement of this initial correlation was later proposed by Janicot and Bestion [17] in 1993. This model is based on the liquid height in the test section H as the turbulence length (e.g. the characteristic length associated to the Nusselt and Reynolds numbers) and the heat exchange area as function of the void fraction in the test section and the injection pipe diameter.

In 2015, Liao et al. [12] developed a new DCC model based on the same dimensionless numbers but an undefined function of the liquid height f(H) to define the turbulence length. This length was then used to calculate the heat exchange area. They decided to fit the correlation using another subset of COSI experiments: the Westinghouse configuration, characterised by a vertical injection. Good results were also shown for the prediction of the condensation in another test facility UPTF (Upper Plenum Test Facility) [18].

In the same year, Ren et al. [19] described the ECCS (Emergency Core Cooling System) facility, which has a test section similar to the COSI one. Once described the phenomenology in the test section, the authors proposed different models based on the same dimensionless

numbers and selected the best-fitting one. Ren et al. defined the same heat exchange area as Liao et al., even if the characteristic length is unknown.

Gaillard and Rodio [20], in 2018, proposed a stratification criterion for single and two-phase flows in presence of a sub-cooled injection. In their paper, a new condensation model at the jet is used for the validation of the criterion. Nevertheless, the authors do not specify which experiments they used to fit the model. In this new correlation, the Froude number, the void fraction and the ratio of the injection diameter over the test section diameter were added to the historical three dimensionless numbers. According to the authors, these parameters take into account the free surface disruption of the jet. Moreover, the heat exchange area is defined as the jet cross section.

In Table 1, the characteristic lengths, reference temperature and temperature difference are summarised for every cited correlation. The reference temperature is the temperature at which the thermodynamic properties of the liquid water are calculated. The temperature difference defines the condensation heat flux $\dot{q}_{cond} = \dot{m}_{cond} \cdot c_p \cdot \Delta T$.

Name	Correlation	Characteristic lengths	T_{ref} and ΔT
Janicot et al. [17]	$Nu = 0.5 \cdot Re$	$l_{Nu} = l_{Re} = H$ $u_{Re} = u_{inj}$ $A_{ex} = d_{jet} \cdot \sqrt{(1-\alpha) \cdot \alpha} \cdot D$	$T_{ref} = unknown$ $\Delta T = T_{sat} - T_{inj}$
Liao et al. [12]	$Nu = 0.245 \cdot Re^{1.1} \cdot Pr^{0.6}$	$l_{Nu} = f(H) \cdot D$ $l_{Re} = d_{inj}$ $u_{Re} = u_{inj}$ $A_{ex} = d_{inj} \cdot f(H) \cdot D$	$T_{ref} = \frac{T_{sat} + T_{inj}}{2}$ $\Delta T = T_{sat} - T_{inj}$
Ren et al. [19]	$Nu = 3.773 \cdot Re$	$l_{Nu} = unknown$ $l_{Re} = d_{inj}$ $u_{Re} = u_{inj}$ $A_{ex} = d_{inj} \cdot l_{Nu}$	$T_{ref} = unknown$ $\Delta T = T_{sat} - T_{inj}$
Gaillard et al. [20]	$Nu = Re \cdot Pr \cdot Fr^{0.5} \cdot \alpha \cdot \frac{d_{jet}}{D}$	$l_{Nu} = l_{Re} = l_{Fr} = H$ $u_{Re} = u_{Fr} = u_{inj}$ $A_{ex} = d_{inj}^2$	$T_{ref} = unknown$ $\Delta T = T_{sat} - T_{inj}$

Table 1 *Jet condensation correlations found in the literature.*

These models are mainly calibrated using different subset data from the same experiment (e.g. COSI) or a very similar one (e.g. ECCS). However, they do not seem consistent with each other. Moreover, the experimental database can be improved and enlarged with other experiments.

In order to better understand the DCC phenomenon induced by a water injection in a circular horizontal pipe and to improve its modelling, three experiments named COSI, TOPFLOW-PTS [21], [22] and UPTF are analysed in this work. These tests were carried out respectively at CEA-Grenoble, HZDR and BMFT-KWU. A reliable and wide experimental database is prepared so that the correlations from the literature can be properly assessed. Eventually, a new correlation is developed and validated.

The paper is organised as follows: in the following section, the experimental databases and their thermal-hydraulic analysis are presented. In Section 3, the experimental database is tested against the physical models from the literature. Section 4 is dedicated to the development and the validation of a new condensation correlation. In Section 5 conclusions are drawn.

2. Experimental database

The correlations found in the literature and reviewed in the introduction must be assessed against experimental data. The assessment process is important to evaluate the predictive capabilities of the models to reproduce the experimental data. If the correlations do not show good results, a new model must be calibrated against the assessment database. The new best-estimate correlation is then tested against an independent database not used to tune the model [23]. This validation phase quantifies the model accuracy in predicting the data when the experimental conditions differ from the calibration ones.

In Table 2, the main characteristics of the experiments are summarised.

	COSI	TOPFLOW-PTS	UPTF
Number of tests	315	42	24

Pressure [MPa]	[2; 7]	[3; 5]	[0.3; 1.5]
Injection temperature [°C]	20, 80	[45; 210]	[30; 40]
Injection mass flowrate [kg/s]	[0.1; 0.6]	[0.7; 2.5]	[10; 160]

Table 2 *Main characteristics of the experiments.*

In the following three sections, the experiments are introduced. Section 2.4. presents the experimental uncertainties. In Section 2.5., a detailed thermal-hydraulic analysis of the experimental database is performed. Finally, Section 2.6 illustrates the methodology used for the quantification of the condensation rate.

2.1. The COSI experiments

The COSI experiment was carried out at CEA Grenoble in the 80s. The goal was to obtain a reliable database to develop a condensation model at the injection [17].

Two test sections were built to simulate the cold leg of a French (Framatome, from now on shortened Fra) and American (Westinghouse, from now on shortened West) nuclear Pressurised Water Reactor (PWR). In Fig. 3, the two configurations consist of:

- A horizontal pipe of 0.118 m in diameter and of 1.4 m in length for Fra and 3.77 m for West;
- An inlet pipe for the steam coming from the boiler and an outlet pipe going to the condenser;
- A vertical pipe to evacuate the water and keep the liquid level constant. This pipe is from now on called downcomer (DC);
- Different injection pipes, welded to the horizontal pipe.

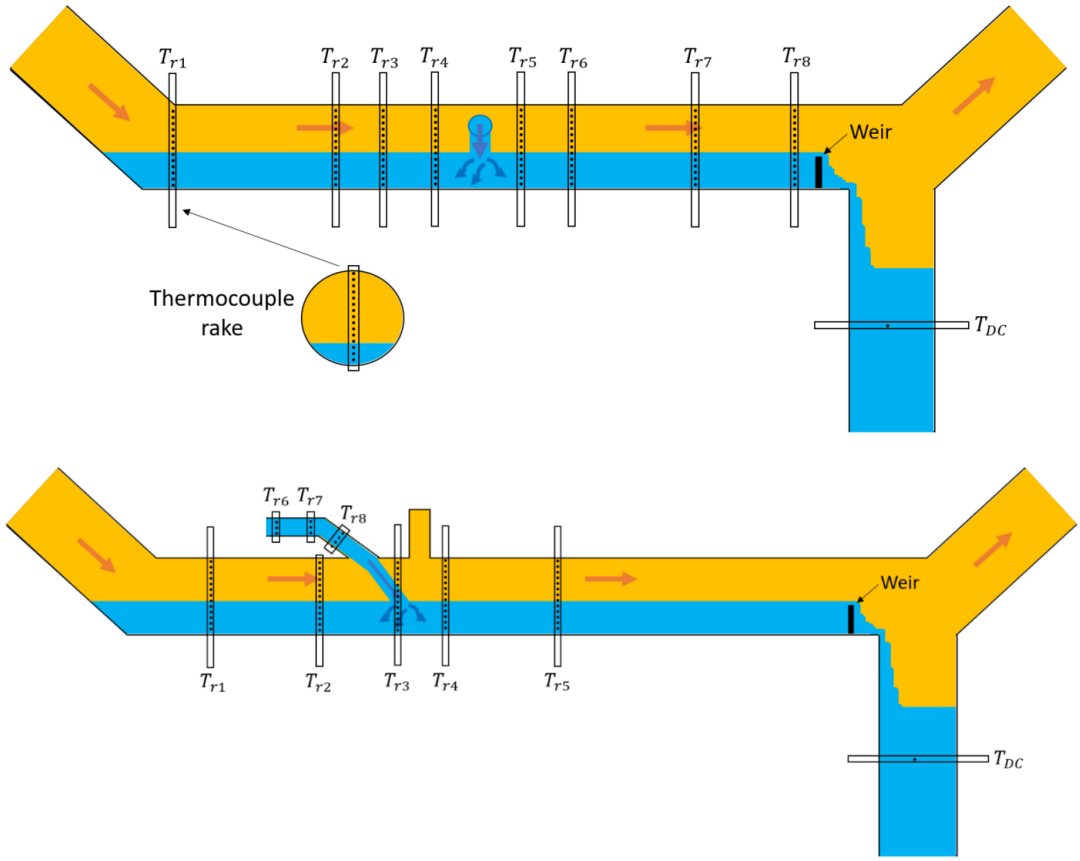

Fig. 3 *Framatome (at the top) and Westinghouse (at the bottom) test sections in the COSI experiment.*

The arrows show the direction of the liquid (blue) and of the steam (orange). In Fig. 3, the steam is depicted co-current with the liquid. Nevertheless, for both configurations, there are tests with steam in co-current and counter-current flow.

The test sections are equipped with the following instrumentation:

- Thermocouple rakes, assemblies of thermocouples used to measure the temperature in precise points in space. The geometry of a rake can be found below the Fra test section in Fig. 3. There are 8 rakes for Fra and 5 for West, of 16 thermocouples each. One injection pipe in the West configuration is also equipped with 3 rakes;
- A thermocouple in the downcomer;
- A weir of adjustable height (0, 0.3, 0.5 times the diameter D for Fra and 0, 0.5 times for West) to keep the liquid level constant in the horizontal pipe.

In Fig. 4 and Table 3, the different injection pipe configurations are shown. The first one being the Fra injection and the two on the right respectively the West injections of type Accumulator (Acc) and High Pressure (HP). Only the HP injection is equipped with thermocouple rakes.

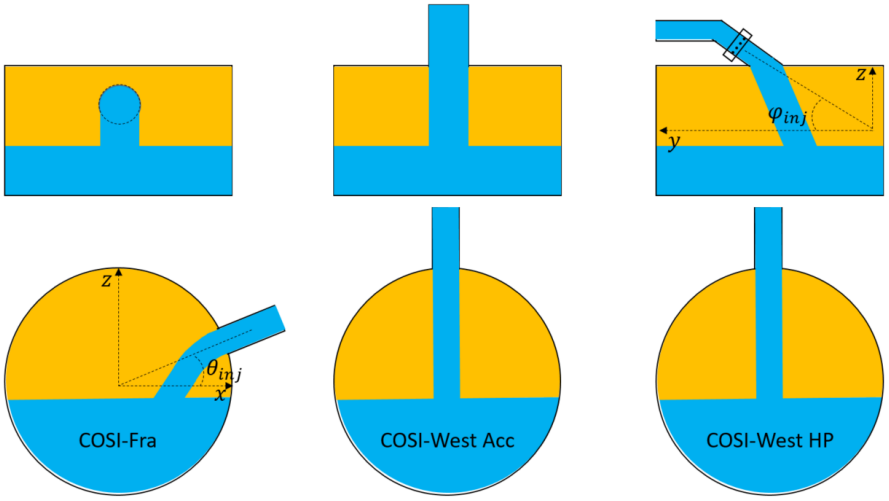

Fig. 4 *Geometrical configurations of the injection pipe in the COSI experiments.*

	COSI-Fra	COSI-West Acc	COSI-West HP
Inclination in the vertical plane θ_{inj}	30	90	90
Inclination in the horizontal plane φ_{inj}	0	0	45
Diameter d_{inj} $[mm]$	22	5.6, 23	38

Table 3 *COSI injection pipe angles and diameters.*

In Fig. 5, a representation of the phenomenology in the COSI experiment is shown. The steam is sent from a boiler into the test section and the phenomenology due to the jet injection is highlighted.

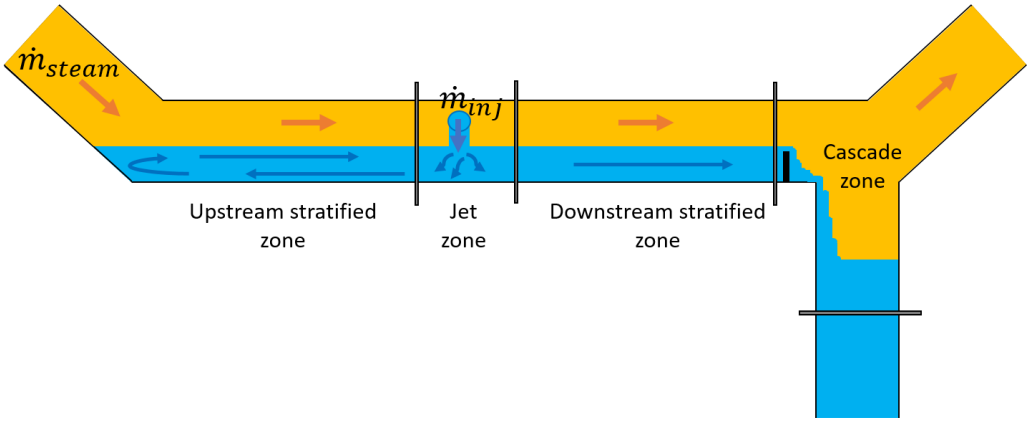

Fig. 5 *Phenomenology in the COSI test section.*

Four different zones can be identified. The injection zone, where the jet impacts the liquid and the steam bubbles may be entrained in the liquid phase. Upstream the jet, large temperature gradients and strong interfacial shears lead to a recirculation zone. Downstream the jet, thermal stratification is observed. The presence of the weir may produce a "standing water" effect, creating a small recirculation zone in the surroundings. After the weir, the water falls in the downcomer generating a cascade.

The COSI database consists of 219 Fra tests and 96 West tests.

2.2. The TOPFLOW-PTS experiments

The TOPFLOW-PTS (Pressurised Thermal Shock) experiment was carried out in Helmholtz-Zentrum of Dresden-Rossendorf (HZDR) in 2010-2012. The goal was to study and better understand the phenomena behind the Pressurised Thermal Shock (PTS), namely the thermal shock phenomena possibly occurring in nuclear reactors due to cold-water injection at high pressure. Data were obtained, mainly to validate Computational Fluid Dynamics (CFD) codes [24].

In Fig. 6, the test section is composed by:

- A pump simulator (PS) with two pipes for water injection and extraction;
- A horizontal pipe of 0.2792 m in diameter and 2.95 m in length;
- An annular space to simulate the DC;
- An injection pipe of 0.0531 m in diameter and welded at 30° in the vertical plane, as shown in Fig. 7.

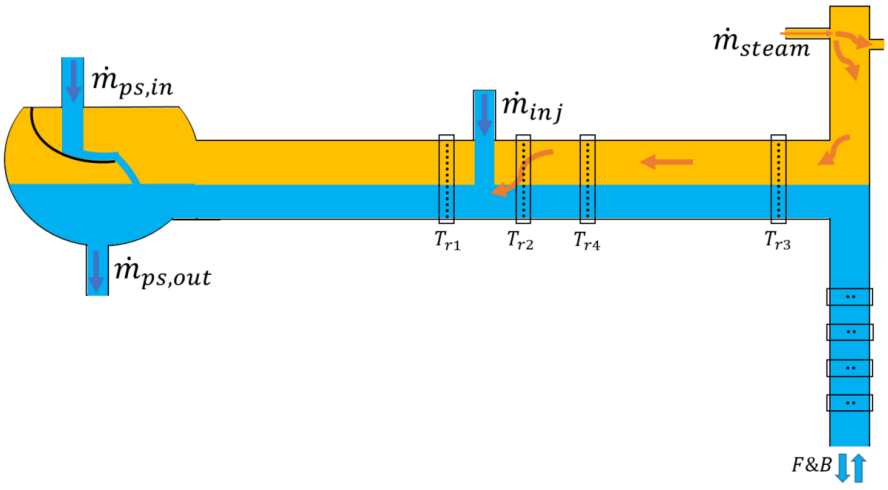

Fig. 6 *TOPFLOW-PTS test section.*

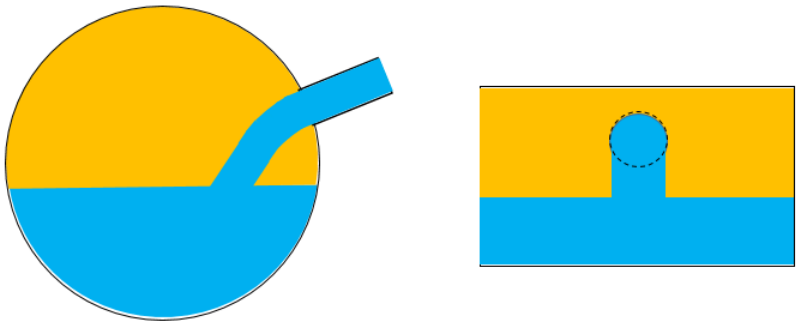

Fig. 7 *TOPFLOW-PTS injection pipe geometrical configuration.*

The test section is equipped with:

- 4 thermocouple rakes of 25 thermocouples each;
- Several thermocouple rakes in the downcomer.

The phenomenology during the experiments is the same as COSI, with the exception of the cascade zone. In TOPFLOW-PTS, the liquid free level is kept constant thanks to a feed & bleed (F&B) system placed at the bottom of the DC. This system extracts a quantity of water equal to the injection and condensed steam mass flowrates, holding always a constant level in the DC.

Two typologies of tests have been realised during the experimental campaign:

1. Steady-state: after a stabilisation transient, the steady-state conditions are reached inside the test section and the jet condensation can be evaluated. Only the final steady-state conditions are registered for 60 seconds. Tests with and without injection/extraction of water in the PS are performed. These tests are indicated as sssw (Steady State Steam Water).
2. Transient state: in this typology, the whole transient is registered from the start of the water injection until the steady-state conditions are obtained. The last 100 seconds of each transient are used to evaluate the jet condensation after a time-averaging. In that period, all the thermal-hydraulic parameters are approximately constant, so that they can be considered as steady-state. The PS is always disabled (i.e. no injection/extraction of water). These tests are indicated as tsw (Transient Steam Water).

The test conditions vary according to different parameters: pressure, steam mass flowrate, free liquid level, jet mass flowrate and temperature.

The TOPFLOW-PTS database consists of 28 sssw tests with PS enabled, 9 sssw tests with PS disabled and 3 tsw tests.

2.3. The UPTF experiments

The UPTF (Upper Plenum Test Facility) experiment has been carried out by Siemens/KWU in the 80s in Germany. It is composed of all the thermal-hydraulic components of a PWR, as described in [18].

Only the tests with a stratified flow in the test section are retained for this analysis, namely UPTF 8, UPTF 25, UPTF 27 and UPTF TRAM C2 6a.

In Fig. 8, the test section is schematised. For the selected tests, it is composed by:

- A PS with no water injection;
- A horizontal pipe of 0.75 m in diameter and 9.48 m in length;
- An annular space to simulate the DC;
- An injection pipe of 0.2225 m in diameter and welded at 60° in the horizontal plane, as shown in Fig. 9.

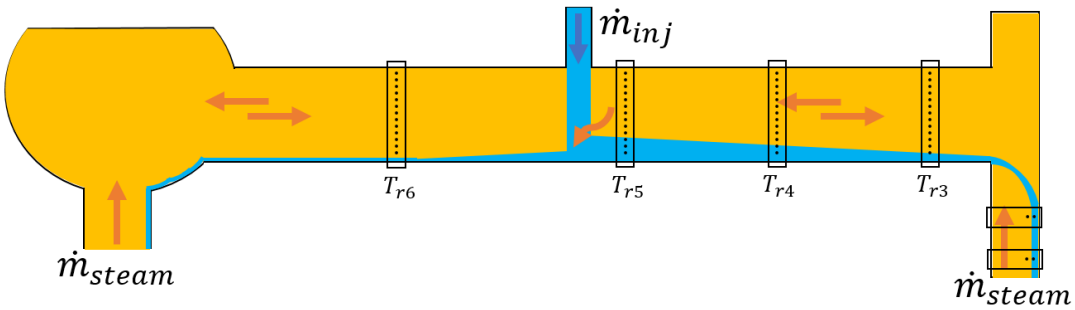

Fig. 8 *UPTF loop II test section.*

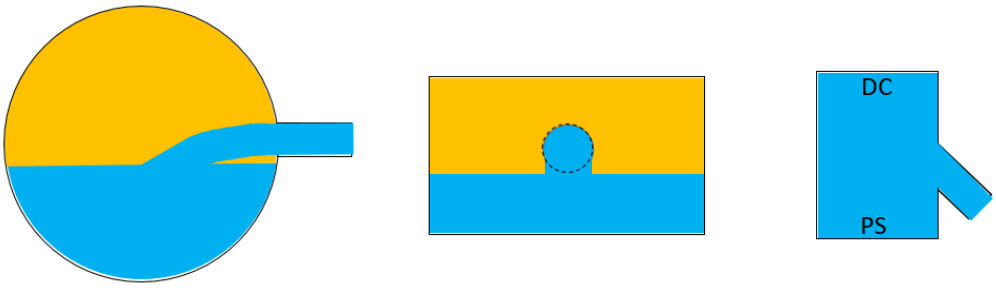

Fig. 9 *UPTF injection pipe geometrical configuration (from the left to the right: perpendicular, side and top view of the test section).*

The test section is equipped with:

- 4 thermocouple rakes of 6 thermocouples each (8 in TRAM configuration);

The phenomenology during the experiments is slightly different with respect to COSI and TOPFLOW-PTS. In UPTF, the liquid flow is directed towards the DC thanks to the injection angle, thus no recirculation zone is present. Moreover, the free level is not maintained constant.

In UPTF 8, 25 and 27, the steam comes from the PS. In TRAM configuration, the PS is full of water and the steam comes from the DC in counter-current direction with respect to the liquid flow.

The UPTF database consists of 24 tests.

2.4. Experimental uncertainties

The experimental uncertainties on the measurements are reported in Table 4. These uncertainties are associated to the geometries of the pipes (both the test section and the injection) and the measurements of temperature, mass flowrate and pressure.

	COSI	TOPFLOW-PTS	UPTF
Diameter	$\pm$0.5 mm	$\pm$0.5 mm	$\pm$0.5 mm
Fluid temperature	$\pm$0.5 °C	$\pm$1 °C	$\pm$2.9 °C
Flowrate	$\pm$0.005 kg/s	$\pm$0.5 %	$\pm$1.5 %
Pressure	$\pm$0.5 %	$\pm$0.5%	$\pm$0.146 bar

Table 4 *Experimental uncertainties.*

2.5. Experimental analysis

The experimental data must be reliable and coherent. A thermal-hydraulic analysis is then performed.

During the experimental campaigns, several tests presented problems such as: no available data, defective instrumentations, incoherent measurements, no sub-cooled injections, no stabilised tests, presence of overheated steam, repeated tests, tests without condensation and calibration tests. Suppressed those tests from the databases, an experimental analysis is carried out on the 198 tests left.

2.5.1. Visualisation and analysis of the jet dynamics

In the TOPFLOW-PTS experiment, a camera is pointing over the jet [22] [25]. The experimental image of a typical sssw test is shown in **Fig. 10**, in which pressure and temperature are representative to those in a reactor.

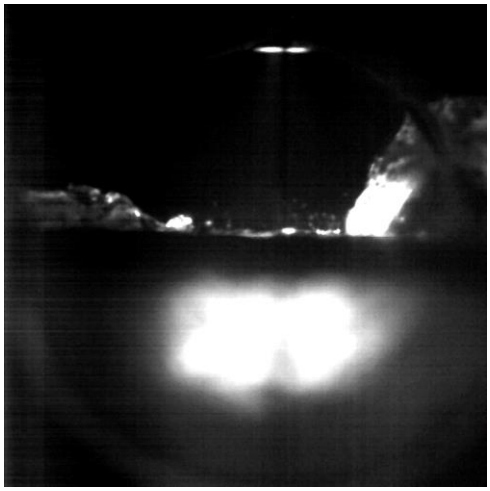

Fig. 10 *Experimental image of a typical TOPFLOW-PTS sssw test injection [25].*

The same main local phenomena described in **Fig. 2** can be found. The jet seems regular and has a quasi-cylindrical shape. At the impact, steam bubbles are entrained in the liquid phase and reflect the light coming from the top of the test section. The lateral rebound is small and the liquid-steam interface does not seem very wavy.

2.5.2. Stratified flow in the injection pipe

In all three experiments (COSI, TOPFLOW-PTS and UPTF), a stratification in the injection pipe was sometimes observed, as shown in Fig. 11. This occurred at low injection mass flowrates.

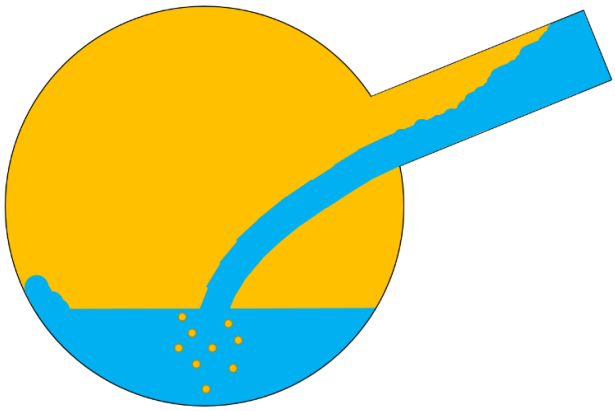

Fig. 11 *Representation of a stratified flow in the injection pipe at 30°.*

This phenomenon affects the injection surface, thus the heat exchange area A_{ex} and the jet velocity u_{inj}. Therefore, these quantities strongly impacting the condensation are either impossible to calculate or, with our simple modelling approach, affected by great uncertainty. It was then decided to exclude the tests with stratified injection from the assessment and validation databases.

In the TOPFLOW-PTS experiment, the experimenters [26] discovered the presence of a stratified flow in the injection pipe for mass flowrates below 1.7 kg/s. Thus, 2 sssw and 1 tsw tests are not considered in our database.

Also in the COSI experiment, a stratification is observed in the HP injection of the West configuration. In this experiment there is no camera, however the thermocouple rake 8 shows a stratified flow. This phenomenon occurs at every injection mass flowrate. This is probably explained by the injection diameter d_{inj} being the biggest one among the possible injection pipe configurations.

The UPTF experimenters wrote in technical reports [27] that a stratified flow may occur in the injection pipe, as shown in Fig. 12.

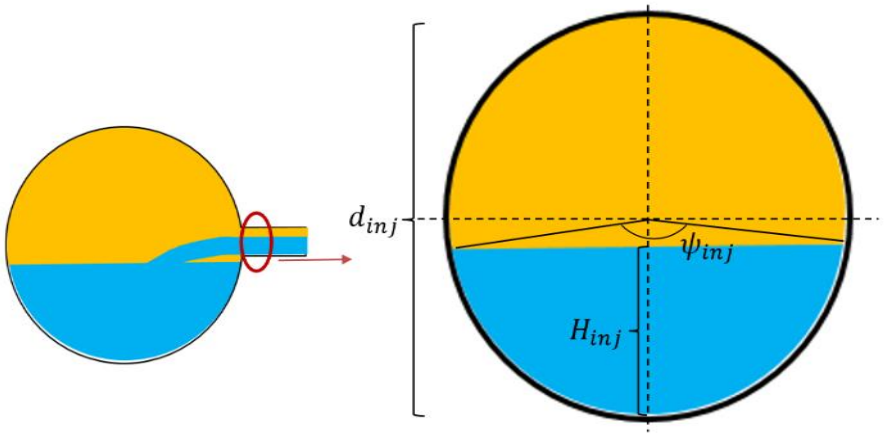

Fig. 12 *Stratified flow in the UPTF injection pipe.*

In the experiment, there is no camera nor thermocouple rakes in the injection pipe. However, the experimenters proposed the Schröder formula [28]. It calculates the liquid height of a two-phase flow inside a low inclined pipe and reads:

$$\begin{cases} \dfrac{\left(\psi_{inj} - \sin\left(\psi_{inj}\right)\right)^3}{\sin\left({}^{\psi_{inj}}/_{2}\right)} = \dfrac{512 \cdot \dot{Q}_{inj}^2 \cdot \rho_{inj}}{g \cdot d_{inj}^5 \cdot \left(\rho_{inj} - \rho_g\right)} \\ H_{inj} = d_{inj} \cdot sin^2\left({}^{\psi_{inj}}/_{4}\right) \end{cases} \quad (1)$$

This formula predicts the occurrence of the stratification phenomenon in all the COSI and TOPFLOW-PTS tests where stratification was experimentally observed. Since Eqn. (1) is validated, it can be used as a stratification criterion. It is applied to the whole database, showing that stratification occurs in 13 UPTF tests and 46 COSI tests. Thus, these 59 tests are not considered in the following analyses. The application range of this study is then limited to fully filled injection pipes. In future works, it would be interesting to take into account the stratification inside the injection pipe and its impact on the modelling of the condensation.

2.5.3. Injection in the liquid

In TOPFLOW-PTS, the camera shows that when the free level is too high the jet enters directly into the liquid.

This phenomenon may occur also in COSI. The tests with the highest weir ($0.6 \cdot D$) are assumed to behave like in Fig. 13.

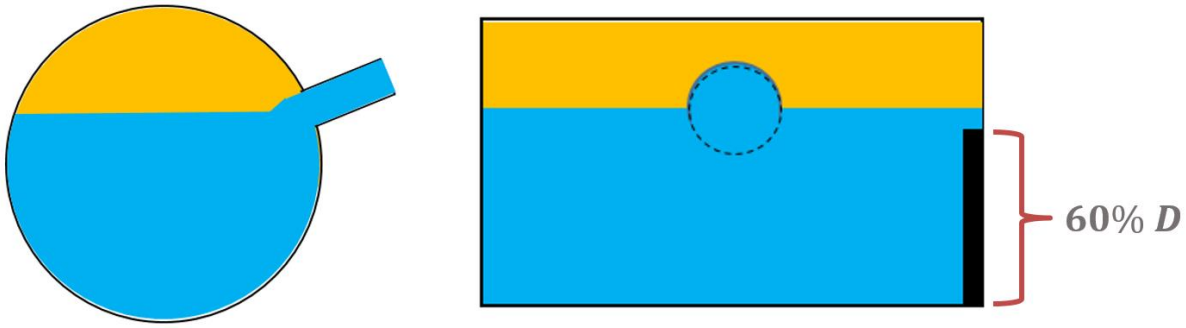

Fig. 13 *Assumed behaviour of COSI tests with a 0.6 weir.*

Those tests are characterised by a short jet, which may lead to small or no condensation rate. Thus, the condensation mass flowrate computation is not reliable in this configuration. 2 tests TOPFLOW-PTS and 6 COSI are then eliminated from the assessment database.

2.5.4. Hot injections in TOPFLOW-PTS

Several TOPFLOW-PTS tests, namely the ones with enabled PS, have a hot water injection. The sub-cooling $\left(T_{sat} - T_{inj}\right)$ is low, between 27 and 80 °C. In these conditions, the calculated

condensation mass flowrate is extremely low and its computation is not reliable due to the strong impact of the experimental uncertainties.

In order to avoid any bias in the assessment of the model, these tests are moved to the validation database.

2.5.5. Reduced database

On the basis of the experimental analysis, it was decided to include the COSI and TOPFLOW experiments in the assessment database. These two experiments are simpler and easier to interpret, so that they are more suitable to assess and develop the condensation model. On the contrary, the UPTF tests are more complex, so that they are used exclusively in the validation phase. As already explained in Section 2.5.3, the TOPFLOW tests with hot injection are also moved to the validation database.

In Table 5, the revised database is shown.

Test	p [MPa]	T_{inj} [°C]	$\dot{m}_{inj}$ $\left[{}^{kg}/_{s}\right]$	Tests in the assessment database	Tests in the validation database
COSI-Fra	2, 7	20, 80	[0.2; 0.6]	73	0
COSI-West	4.2, 5.6, 7	20	[0.06; 0.4]	29	0
TOPFLOW-PTS sssw	3, 5	[110; 220]	[0.7; 2.5]	6	11
TOPFLOW-PTS tsw	5	[110; 220]	[0.7; 2.5]	2	0
UPTF	[0.3; 1.5]	[29; 39]	[10; 161]	0	7
Total number of tests				110	18

Table 5 *Reduced database after the experimental analysis.*

At the end of the thermal-hydraulic analysis, the assessment database is composed of 110 tests and the validation database of 18 tests. The experimental conditions range between 0.3 and 7 MPa for the pressure, 0.2-161 kg/s for the injection flowrate and between 20 and 220 °C for the injection temperature.

2.6. Methodology for the quantification of the condensation rate

As already seen in the literature, the condensation in the jet region is modelled through dimensionless numbers. In order to calculate these numbers and properly assess the

correlations in Table 1, the following physical quantities must be evaluated from the experimental data:

1. The liquid level height in the test section;
2. The mean liquid temperature $\bar{T}_{r,i}$ from the rake of thermocouples;
3. The condensation mass flowrate at the injection $\dot{m}_{cond}$.

A methodology for each of these quantities is here below presented.

2.6.1. Evaluation of the liquid level height and of the mean liquid temperature

For the calculation of the condensation mass flowrate and the heat exchange area, respectively the mean liquid temperature of each rake and the liquid level height in the test section must be estimated (e.g. the interface between the two phases must be identified).

The impact of the jet in the circular test section creates waves at the interface between the gas and liquid phases.

In the TOPFLOW-PTS experiment, the thermocouple temperature profiles in time are recorded and plotted in Fig. 14. There, the normalised temperature (with respect to the saturation temperature plus a random small constant ξ) is plotted against the time. Three thermocouples are shown: one in the steam (in yellow) at the saturation temperature, one in the liquid (in light blue) and one at the interface (in grey).

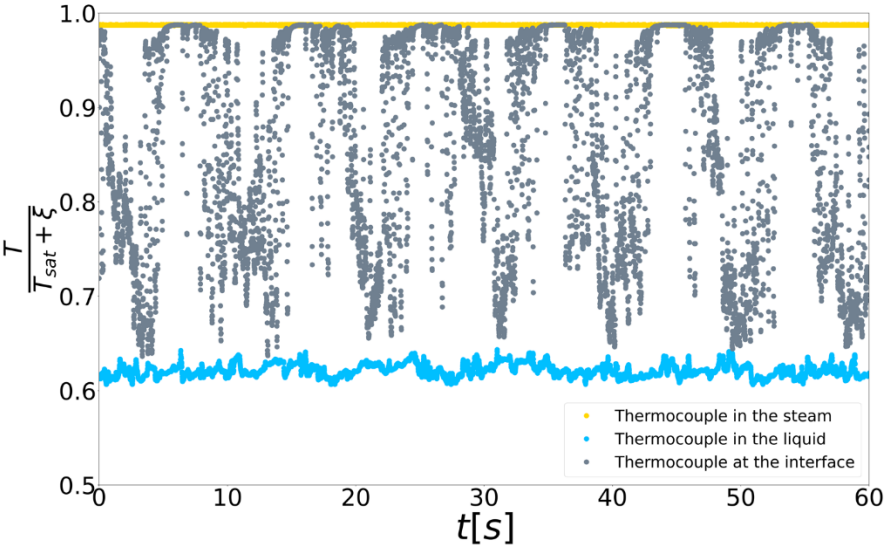

Fig. 14 *Typical temperature profiles in time in a TOPFLOW-PTS test.*

The thermocouple at the interface is in the steam and it is wetted regularly by the waves. Thus, it is not representative of the liquid temperature.

A typical rake time-averaged temperature profile is shown in Fig. 15. There, the normalised temperature is plotted against the dimensionless height of the thermocouple in the test section. The black line marks the saturation temperature T_{sat}, the red one T_{sat} – 5 °C.

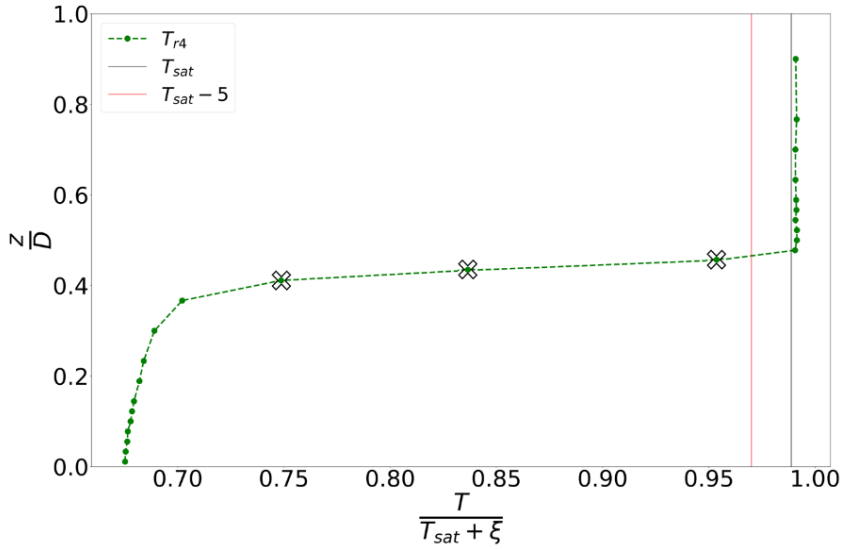

Fig. 15 *Typical time-averaged temperature profile of a rake in a TOPFLOW-PTS test.*

Three different zones can be identified. All the thermocouples below z/D=0.4 are most likely in the liquid. The other thermocouples are either positioned at the liquid-steam interface (e.g. the zone in the middle, 0.4 < z/D < 0.5 and $T < T_{sat}$ - 5 °C) or in the steam (e.g. the right zone, where the temperature is higher than T_{sat} - 5 °C). In particular, three thermocouples are identified at the liquid-steam interface (black crosses in Fig. 15) since they are characterised by significant temperature fluctuations in the experiment.

Based on these experimental observations on the TOPFLOW-PTS tests, a criterion to identify the thermocouples in the liquid and the liquid-steam interface has been developed and validated. Starting from the bottom of the rake, the first thermocouple is always supposed in the liquid. Proceeding up the rake, the increase of temperature between two successive thermocouples is compared to the sub-cooling of the thermocouple (i.e. the difference between the saturation and the thermocouple temperature). If the temperature increase is larger than 80 % of the sub-cooling, then the thermocouple is considered at the liquid-steam interface. All other thermocouples at higher *z/D* are then supposed in the steam and neglected when evaluating the average liquid temperature of the rake.

The free level in the test section is computed as the halfway distance between the last thermocouple in the liquid and the first one detected at the interface.

The COSI and the UPTF experiments have very similar time-averaged temperature profiles to the TOPFLOW-PTS one in Fig. 15. However, the time evolution of the temperatures are not available. The new developed criterion is then applied and the thermocouples in the liquid are identified.

In the end, for all the experiments, the rake mean liquid temperature is calculated. Assuming a uniform liquid velocity field, the weighted mean of those temperatures with the associated surfaces (shown in Fig. 16) gives the mean liquid temperature:

$$\bar{T}_r = \frac{\sum_{k=1}^{k=last\ TC\ in\ the\ liquid} T_k \cdot S_k}{\sum_{k=1}^{k=last\ TC\ in\ the\ liquid} S_k} \quad (2)$$

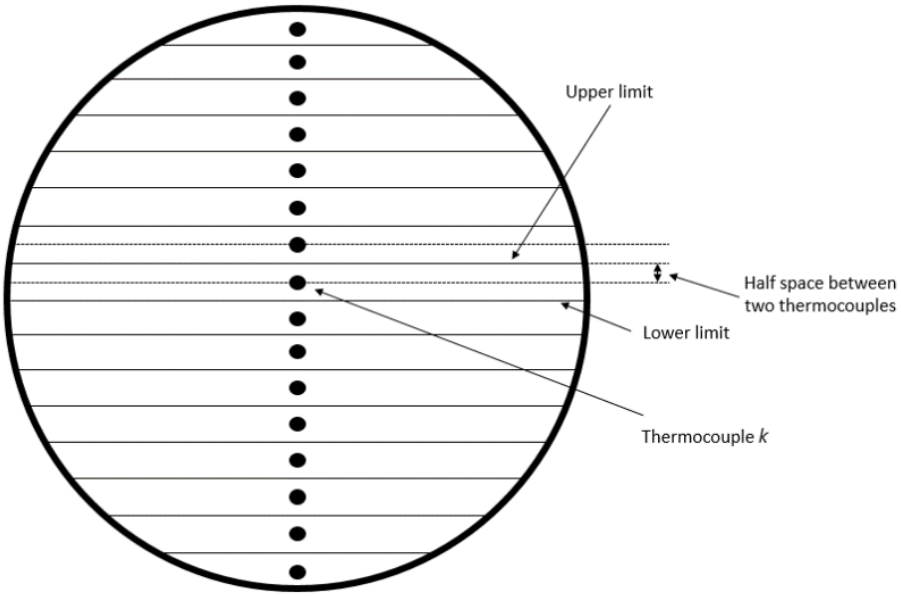

Fig. 16 *Thermocouple associated surfaces estimation for a COSI rake.*

Several experimental uncertainties (see Table 4) may influence the calculation of the mean liquid temperature. A Monte-Carlo propagation of these uncertainties is performed to estimate the experimental uncertainty on the mean liquid temperature. Two main hypothesis are made. First, no uncertainty on which is the last TC in the liquid is considered. Second, the uncertainty on the liquid height in the test section H is equal to the half space between the last thermocouple in the liquid and the first in the steam.

The rake mean liquid temperature is then estimated to have an uncertainty up to $\pm$6 °C for COSI, $\pm$4 °C for TOPFLOW-PTS and $\pm$3.5 °C for UPTF experiments.

2.6.2. Quantification of the condensation mass flowrate

Historically, the correlations based on the COSI experiments were obtained calculating the condensation mass flowrate applying an energy balance over the whole COSI test section (from the jet to the thermocouple in the DC). Defining the control volume in this way, the condensation due to the cascade and to the stratification is accounted as due to the jet. To separate the effects, a new methodology for the quantification of the jet condensation has been developed. The condensation mass flowrate is quantified defining a control volume (shown in Fig. 17) between the injection and a thermocouple rake whose mean liquid temperature is calculated according to the previous section.

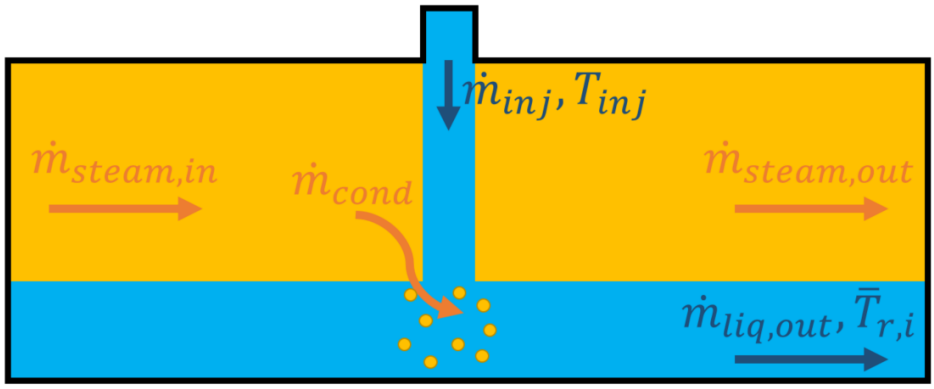

Fig. 17 *Control volume between the injection and a thermocouple rake.*

Applying an energy balance to the control volume in terms of enthalpy, the steam mass flowrate condensing in the liquid phase is computed as:

$$\dot{m}_{cond} = \dot{m}_{inj} \cdot \frac{\bar{\imath}_{r,i} - i_{inj}}{i_{g,sat} - \bar{\imath}_{r,i}} \tag{3}$$

Assuming that the condensation in the stratification zone is negligible, due to the reduced test section length between the injection and the DC, Eqn. (3) can be applied:

- Between the jet and the rake 8 for COSI-Fra (5 for COSI-West), to quantify the condensation occurring at the jet.
- Between the rake 8 for COSI-Fra (5 for COSI-West) and the thermocouple in the DC, to quantify the condensation at the cascade.

In this way, the condensation term at the cascade can be compared to the jet one (Fig. 18).

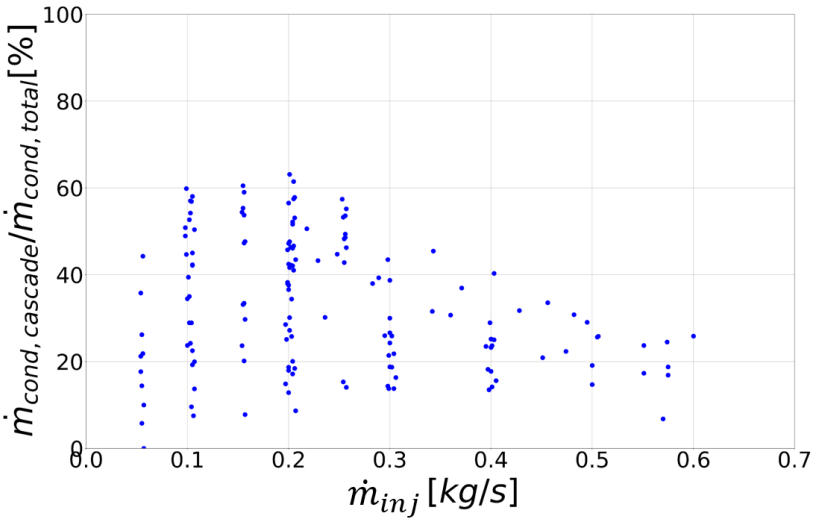

Fig. 18 *Percentage of the condensation due to the cascade over the global condensation for the COSI experiments.*

The condensation at the cascade can go up to 60% of the total condensation for low injection mass flowrates. This proves that the choice of the control volume, to compute the jet condensation mass flowrate, is of great importance.

The same local energy balance is applied to TOPFLOW-PTS and UPTF. In these experiments, the stratified condensation is not negligible anymore. Thus, the condensation mass flowrate is calculated between the jet and rake 4 for TOPFLOW-PTS and rake 5 for UPTF.

3. Assessment of selected correlations from the literature

The accuracy associated to a thermal-hydraulic correlation must be quantified in a rigorous manner. It can be estimated through some statistical indicators which assess the model ability to calculate the output physical quantity. In this work, the indicators proposed in [29] are adopted.

3.1. Statistical indicators

From the comparison between experimental and calculated data, a relative and absolute residual can be defined. For an output quantity *z*, they read respectively:

$$\begin{cases} \varepsilon_{z,rel} = \dfrac{1}{n} \cdot \displaystyle\sum_{i=1}^{n} \dfrac{z_{calc,i} - z_{exp,i}}{z_{exp,i}} \cdot 100 \\ \left|\varepsilon_{z,rel}\right| = \dfrac{1}{n} \cdot \displaystyle\sum_{i=1}^{n} \left|\dfrac{z_{calc,i} - z_{exp,i}}{z_{exp,i}}\right| \cdot 100 \end{cases} \quad (4)$$

$$\begin{cases} \varepsilon_{z,abs} = \dfrac{1}{n} \cdot \displaystyle\sum_{i=1}^{n} z_{calc,i} - z_{exp,i} \\ \left|\varepsilon_{z,abs}\right| = \dfrac{1}{n} \cdot \displaystyle\sum_{i=1}^{n} \left|z_{calc,i} - z_{exp,i}\right| \end{cases} \quad (5)$$

where n is the number of tests.

In Eqns. (4) and (5), the mean and standard deviation of the first indicator (without absolute value) give respectively the accuracy and the precision of the model while the mean of the second one (with modulus) measures the average error of the prediction.

To measure the goodness of fit, the coefficient of determination R^2 defined in [30] is selected. The higher the prediction quality of the model is, the closer the coefficient is to one.

3.2. Results of the assessment

In Table 1, the physical models are shown together with their characteristic lengths.

In order to quantify their performances, these correlations are tested against the new revised assessment database. When the reference temperature T_{ref} is unknown, it is supposed to be equal to the Liao et al. one. In Table 6, the residuals are quantified with Eqn. (5).

Name	$\left\|\varepsilon_{T,abs}\right\|_{COSI}$ [°C]	$\left\|\varepsilon_{T,abs}\right\|_{TOPFLOW-PTS}$ [°C]
Janicot et al.	53	87
Liao et al.	48	86
Gaillard et al.	72	20
Ren et al.	71	89

Table 6 *Correlation errors against the new revised database.*

The models do not show good results.

The Janicot and Liao correlations overestimate the condensation mass flowrate in both the COSI and TOPFLOW-PTS experiments, resulting in hotter calculated mean liquid temperatures $\overline{T}_r$. This may be due to the wrong control volume (e.g. from the jet to the DC) used to quantify the experimental condensation mass flowrate in the two articles. These flowrates were overestimated since the condensation due to the cascade and to the stratification was accounted to the jet.

The Ren et al. model behaves similarly, overestimating the jet condensation. This may be due to the same reason (e.g. the wrong definition of the control volume over the ECCS test section).

These three models show the worst results when applied to the TOPFLOW-PTS database, showing on average an absolute residual of ~90 °C. These poor predictions may be due to the model not scaling well with bigger jet dimensions, which characterise the TOPFLOW-PTS injection.

The Gaillard et al. correlation systematically underestimates the condensation. However, this model performs the best against the TOPFLOW-PTS tests. This may be due to the shape factor $\frac{d_{jet}}{D}$, which takes into account the bigger jet dimension with respect to the COSI one.

4. Development and validation of a new jet condensation model

In Section 3, the correlations found in the literature have been assessed against our experimental database. The condensation modelling through the Nusselt number, as often suggested in the literature, is not satisfactory. Thus, a new approach is presented in this section.

4.1. Modelling of the jet as an heat exchanger

The jet can be seen as a concentric heat exchanger. The heat exchange between the liquid and the steam varies with the position along the jet length. In Fig. 19, the primary side consists of

the cold liquid that enters at T_{inj} and leaves at $\bar{T}_r$ (as already seen in Fig. 17). The secondary side is represented by the steam, at saturation temperature.

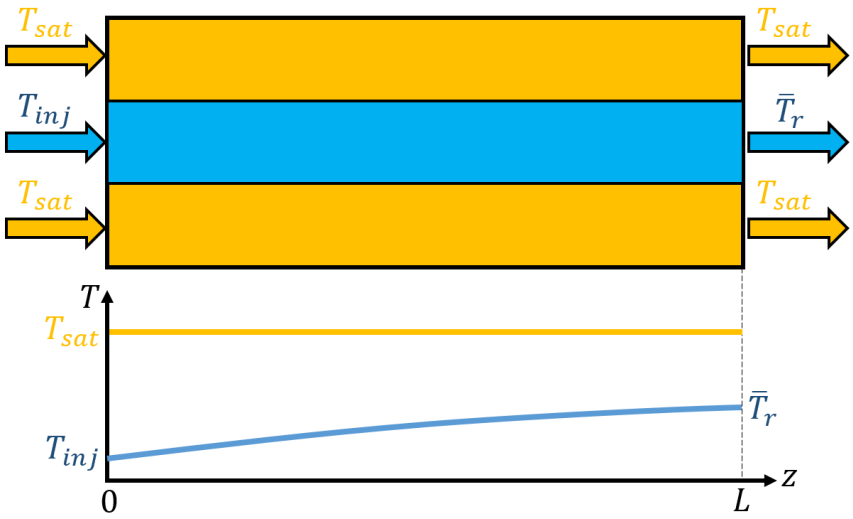

Fig. 19 *Visualisation of the jet as a heat exchanger.*

Thus, the temperature difference representative of the heat exchange at the jet is the logarithmic mean temperature difference that reads:

$$\Delta T_{ln} = \frac{\Delta T_{in} - \Delta T_{out}}{ln\left({}^{\Delta T_{in}}/_{\Delta T_{out}}\right)} = \frac{\bar{T}_r - T_{inj}}{ln\left({}^{(T_{sat} - T_{inj})}/_{(T_{sat} - \bar{T}_r)}\right)} \tag{6}$$

The condensation heat flux can be then written as:

$$\dot{q}_{cond} = \dot{m}_{cond} \cdot i_{lg} = h \cdot A_{ex} \cdot \Delta T_{ln} \tag{7}$$

4.2. Modelling of the heat transfer area

The heat transfer area is difficult to model due to the turbulent and chaotic nature of the physical phenomenon. In Fig. 20, different heat exchange areas are illustrated for a vertical injection.

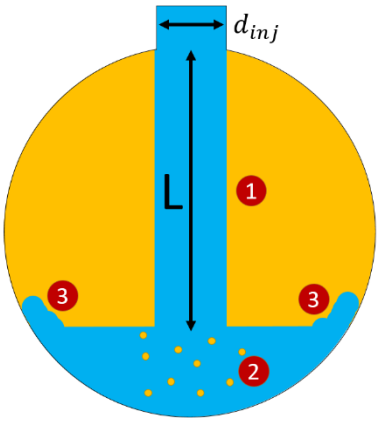

Fig. 20 *Heat exchange areas for a vertical injection.*

As already observed in Fig. 10, three different zones can be found:

1. A cylindrical zone, from the injection pipe outlet to the liquid phase;
2. An entrainment zone, due to the impact of the jet in the liquid;
3. A rebound zone, where the liquid is above the free level and the kinetic energy is transformed in potential energy.

As suggested in [31], we suppose that most of the condensation occurs in the first zone. Due to this hypothesis, the heat transfer area can be approximated as:

$$A_{ex} = \pi \cdot d_{inj} \cdot L \tag{8}$$

For injection angles lower than 90°, the jet length *L* can be estimated using the Clausnitzer & Hager formula [32] that allows to compute the lower trajectory (or lower nappe) of the jet. The lower nappe is then described by the following equation in the reference system (x', y') in Fig. 21:

$$y' = \frac{1}{3} \cdot x' \cdot Fr^{-0.8} + \frac{1}{4 \cdot d_{inj}} \cdot x'^2 \cdot Fr^{-1.6} \tag{9}$$

The Froude number is defined by the velocity u_{inj} and the diameter d_{inj} of the jet. Thus, the trajectory is dependent on the jet geometry and kinetic energy. A faster and thinner jet (high Froude) describes a longer nappe.

The Clausnitzer & Hager correlation was originally developed for horizontal injection pipes at atmospheric pressure. Its application for inclined pipes at high pressure is validated thanks to

the TOPFLOW-PTS tests images. In Fig. 21, the dimensionless experimental nappes (in light blue) of a TOPFLOW-PTS test are plotted. The lower nappe (in green) is computed applying Eqn. (9) and rotating it counter clockwise of the injection angle θ_{inj}, showing really good results. The centred trajectory of the jet (in black) is then obtained translating the parabola of $d_{inj}/_2$ towards the jet centre of symmetry and adding the segment between the injection pipe exit and the parabola first point (the thin black segment).

This rotated Clausnitzer & Hager formula is validated for all the TOPFLOW-PTS test images and is then applied to the whole database.

The jet length is finally obtained integrating the centred trajectory of the jet.

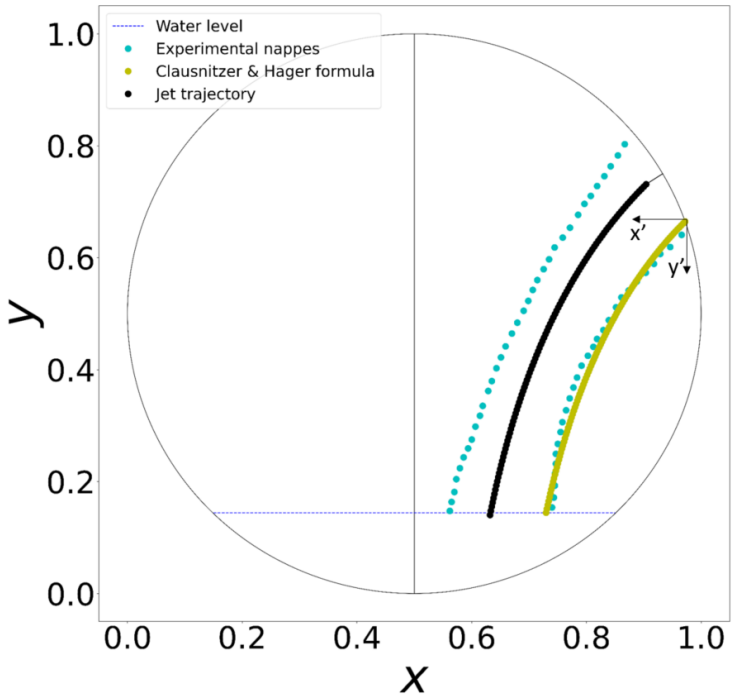

Fig. 21 *Application of the Clausnitzer & Hager formula to compute the lower nappe of the jet and its centred trajectory in a TOPFLOW-PTS test.*

4.3. Modelling of the condensation potential

The heat exchanger condensation potential R is defined as:

$$R = \frac{\bar{T}_r - T_{inj}}{T_{sat} - T_{inj}} \tag{10}$$

It measures how much the cold jet is exploited to condense the steam. If R=1, the cold jet condenses all the steam possible so that it reaches the saturation temperature. If R=0, the jet condenses no steam.

The condensation potential in Eqn. (10) can be analytically modelled adapting the approach proposed for boiling in [33] and [34] to the condensation [35]. Combining Eqn. (7) with Eqn. (3) and using the ratio between the heat exchange and the jet cross sectional areas:

$$\frac{A_{ex}}{A_{inj}} = \frac{\pi \cdot d_{inj} \cdot L}{\pi/4 \cdot d_{inj}^2} = 4 \cdot \frac{L}{d_{inj}} \tag{11}$$

The liquid temperature difference in the heat exchanger can be written as:

$$\bar{T}_r - T_{inj} = \frac{q''_{cond}}{\dot{G}_{inj} \cdot c_{p,ref}} \cdot 4 \cdot \frac{L}{d_{inj}} \cdot \frac{i_{g,sat} - \bar{\imath}_{r,i}}{i_{lg}} \tag{12}$$

Supposing the characteristic lengths of Nusselt and Reynolds numbers to be equal, the Stanton number can be defined using the heat flux in Eqn. (7) as:

$$St = \frac{q''_{cond}}{\dot{G}_{inj} \cdot c_{p,ref}} \cdot \frac{\rho_{inj}}{\rho_{ref}} \cdot \frac{1}{\Delta T_{ln}} \tag{13}$$

Thus, combining Eqns. (12) and (1):

$$\bar{T}_r - T_{inj} = St \cdot \frac{\rho_{ref}}{\rho_{inj}} \cdot \Delta T_{ln} \cdot 4 \cdot \frac{L}{d_{inj}} \cdot \frac{i_{g,sat} - \bar{\imath}_{r,i}}{i_{lg}} \tag{14}$$

Eqn. (14) can be put in the definition of the condensation potential. Considering that the argument of the logarithm in Eqn. (6) can be rewritten as $1/(1-R)$, it follows:

$$R = 1 - exp\left(-4 \cdot St \cdot \frac{\rho_{ref}}{\rho_{inj}} \cdot \frac{i_{g,sat} - \bar{\imath}_r}{i_{lg}} \cdot \frac{L}{d_{inj}}\right) \tag{15}$$

For simplicity, Eqn. (15) can be rewritten as:

$$\begin{cases} R = 1 - exp\left(-4 \cdot \eta \cdot \dfrac{L}{d_{inj}}\right) \\ \eta = St \cdot \dfrac{\rho_{ref}}{\rho_{inj}} \cdot \dfrac{i_{g,sat} - \bar{\imath}_r}{i_{lg}} \end{cases} \tag{16}$$

From Eqn. (16), the condensation potential is then a function of the geometrical feature of the jet $\frac{L}{d_{inj}}$ (also called shape parameter) and a coefficient η. In Fig. 22, R is plotted against the shape parameter for both the assessment and the validation databases.

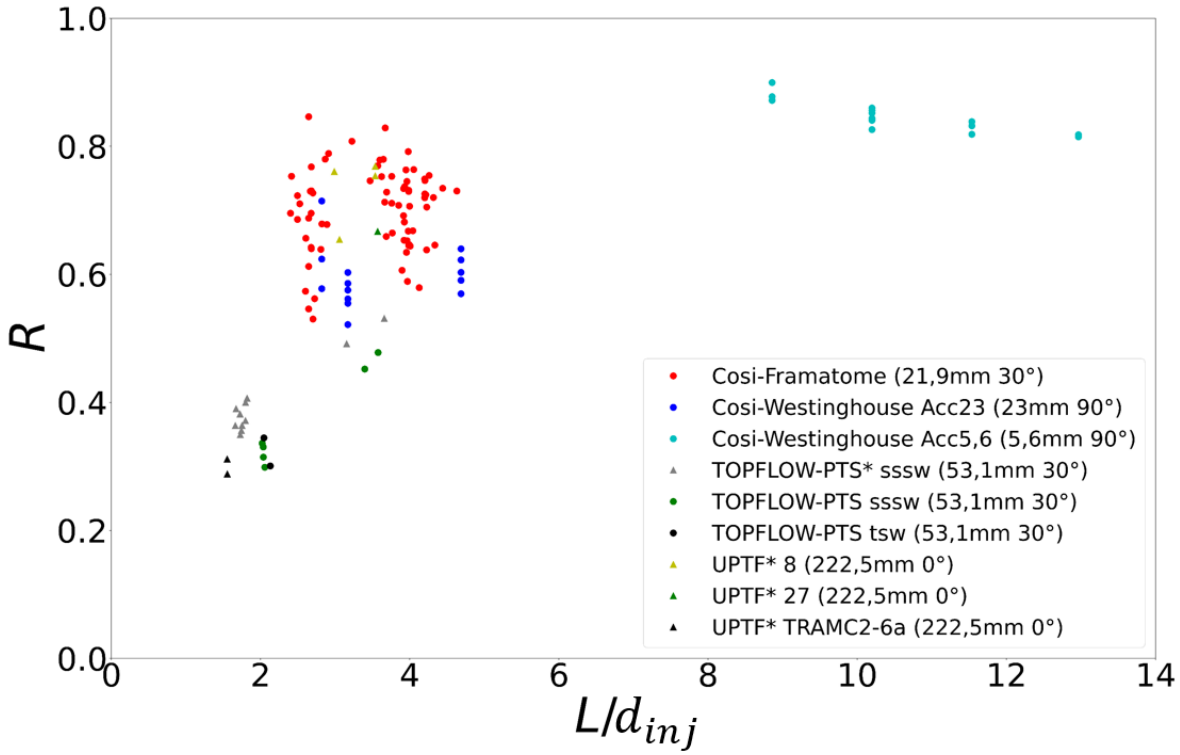

Fig. 22 *Condensation potential R plotted against the jet length over diameter ratio. The triangles are the validation tests (also marked as * in the legend).*

It can be observed that the condensation potential R seems to depend exponentially to the shape parameter. The longer and thinner the jet is, the closer the condensation potential is to one.

The exponential dependence analytically derived in Eqn. (15) is suitable to fit the experimental data. Properly assessing a model for η allows us to interpolate the data through Eqn. (16).

4.4. Modelling of η

The η can be modelled through different dimensionless parameters. After a long work of analysis, the best-suited ones were identified as: the steam potential Nusselt, the injection Reynolds and the reference Prandtl dimensionless numbers. The correlation is introduced here below:

$$\eta = \theta_0 \cdot Nu_{pot}^{\theta_1} \cdot Re_{inj}^{\theta_2} \cdot Pr_{ref}^{\theta_3} \quad (17)$$

where the steam potential Nusselt number is defined as:

$$Nu_{pot} = \frac{\dot{m}_{vap} \cdot i_{lg} \cdot l_{c,Nupot}}{A_{ex} \cdot k_{ref} \cdot (T_{sat} - T_{inj})} \quad (18)$$

It is defined as potential since it is calculated as if all the steam flowrate reaching the jet condensed, with the maximum temperature difference possible (i.e. $T_{sat} - T_{inj}$). It is important to model the effect of the steam flowrate on the condensation, as observed for the DCC in other configurations (e.g. [36] [37]).

The characteristic lengths are summarised in Table 7.

Scales	Definition
Reynolds velocity	u_{inj}
Characteristic lengths	$l_{Nu,pot} = l_{Re} = d_{inj}$
Reference temperature	$T_{ref} = \frac{T_{sat} + T_{inj}}{2}$

Table 7 *Characteristic lengths for the new correlation.*

4.5. Development of the correlation

The coefficients θ, introduced in Eqn. (17), are simultaneously optimised using the calibration methodology proposed in [29]. This procedure is applied to the assessment database.

The correlation then reads:

$$\eta = 0.014 \cdot Nu_{pot}^{0.58} \cdot Re_{inj}^{-0.33} \cdot Pr_{ref}^{-1.2} \quad (19)$$

The coefficient of determination R^2 (see Section 3.1.) associated to this model is equal to 0.82. Thus, the correlation ability to reproduce the experimental data is good.

Eqn. (19) leads to good predictions, as shown in Fig. 23 and Table 8 where the errors are quantified and summarised.

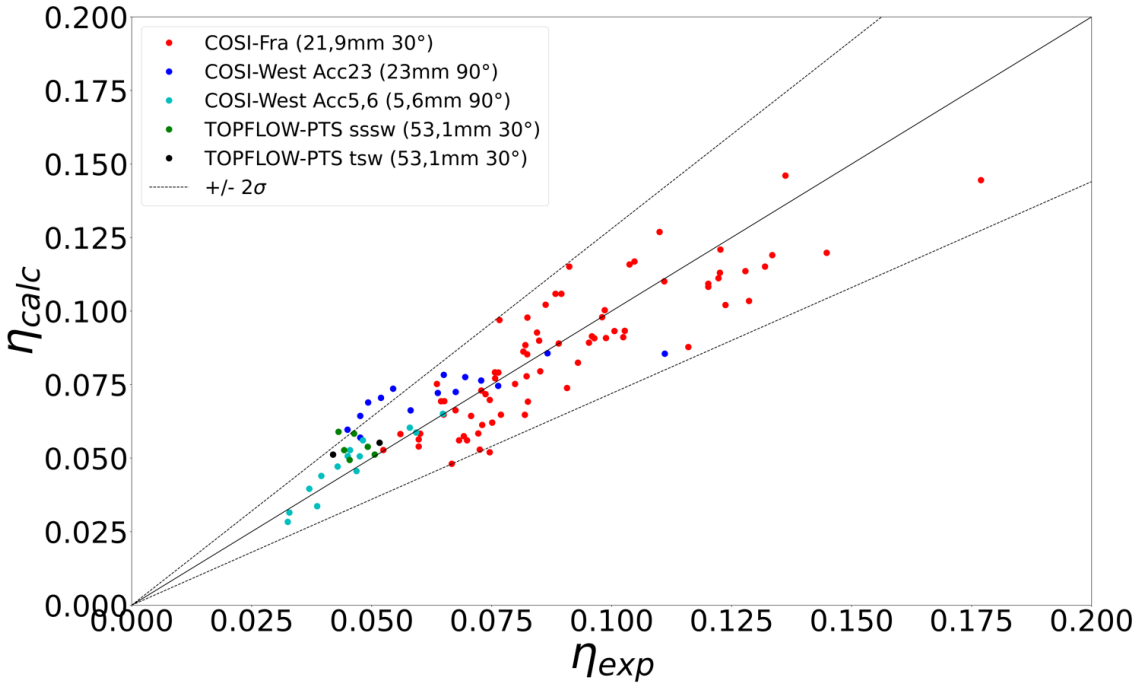

Fig. 23 *Fitting of the new condensation correlation over the assessment database.*

	Mean [%]	Standard deviation σ [%]	Min [%]	Max [%]
$\varepsilon_{\eta,rel}$	1.2	15.4	-30.3	40
$\lvert\varepsilon_{\eta,rel}\rvert$	12.3	-	-	-
$\lvert\varepsilon_{\eta,rel}\rvert_{COSI}$	12	-	-	-
$\lvert\varepsilon_{\eta,rel}\rvert_{TOPFLOW-PTS}$	16.3	-	-	-

Table 8 *Relative error prediction on η for the new correlation.*

The prediction of η is centred with a dispersion of 2σ = 30.8 %. The relative error values show good results. The experiment-model discrepancy is on average equal to 12.3 %.

Once calculated the η with the model in Eqn. (19), Eqns. (16) and (10) can be applied to derive the mean liquid temperature $\bar{T}_r$.

In Fig. 24, the experimental temperatures are plotted against the calculated temperatures. Two error bands in red show an error of $\pm$30 °C.

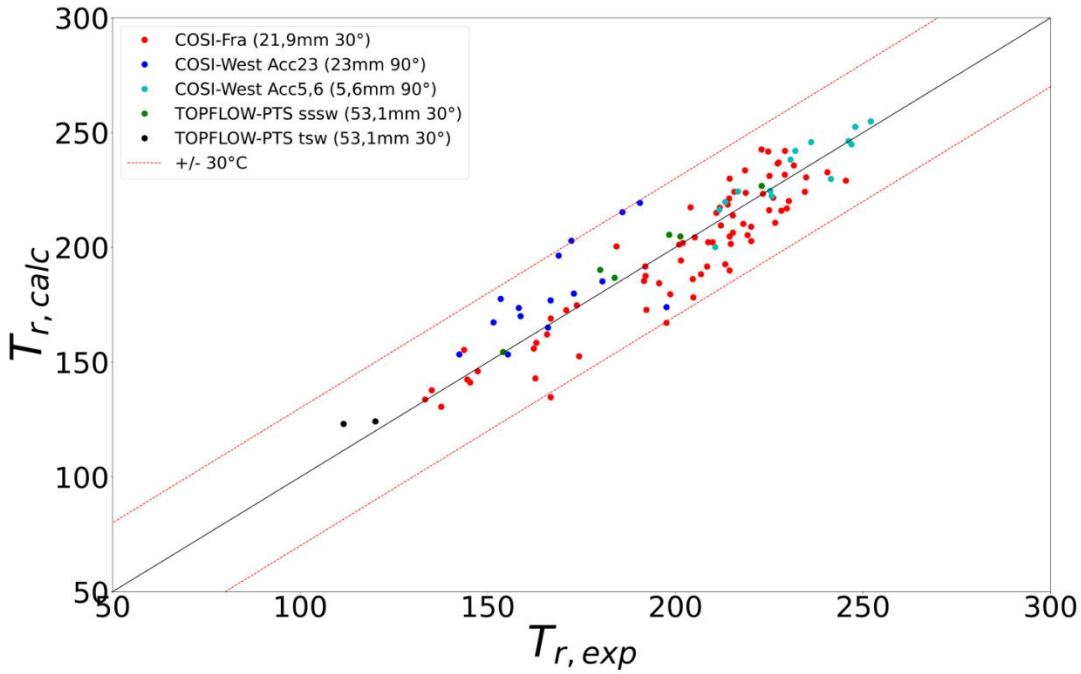

Fig. 24 *Prediction of the mean liquid temperature against the assessment database.*

The indicators in Eqn. (5) are computed with respect to the assessment database and presented in Table 9.

	Mean [°C]	Standard deviation σ [°C]	Min [°C]	Max [°C]
ε_T	-1	13	-32	31
$\lvert\varepsilon_T\rvert$	10	-	-	-
$\lvert\varepsilon_T\rvert_{COSI}$	10	-	-	-
$\lvert\varepsilon_T\rvert_{TOPFLOW-PTS}$	5	-	-	-

Table 9 *Absolute errors on the temperature with respect to the assessment database.*

The model gives centred predictions with a dispersion of $2\sigma = 26$ °C. The min and max are almost the same, not showing a trend of the model to systematically under- or over-predict the condensation. Moreover, the mean absolute errors (both for COSI and TOPFLOW-PTS) are comparable to the measurement errors quantified in Section 2.6.1., emphasising the model capability to reproduce the experimental data.

4.5. Validation of the correlation

The mean liquid temperature $\bar{T}_r$ is calculated for the validation database, composed by 7 UPTF tests and 11 TOPFLOW-PTS tests with a hot injection. In Fig. 25, the experimental temperatures are plotted against the calculated temperatures.

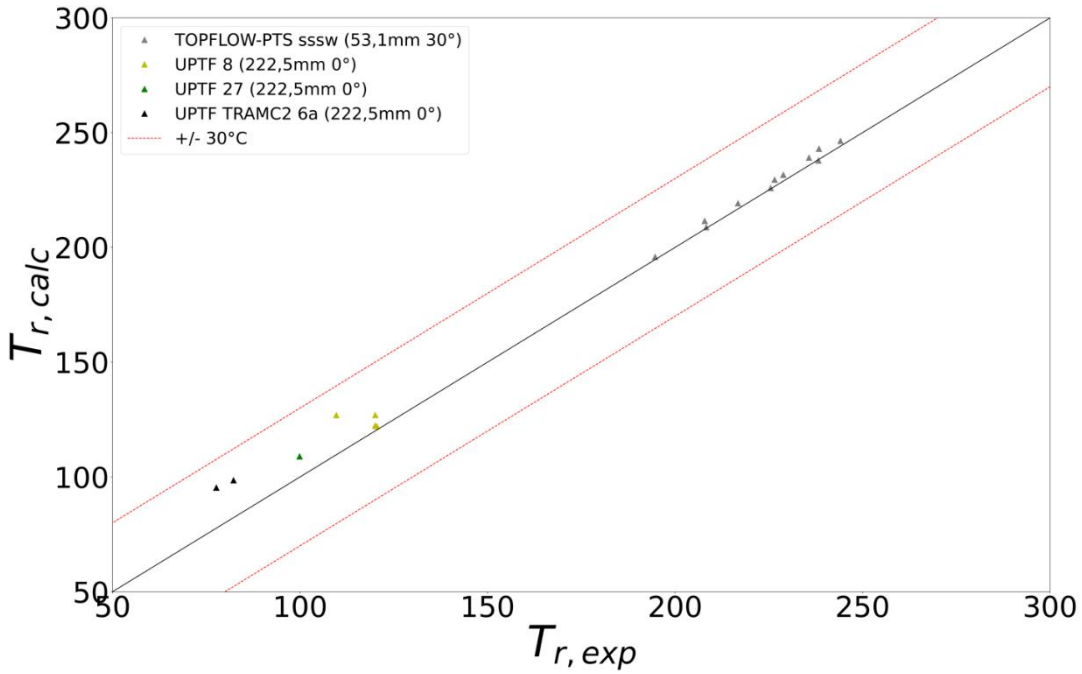

Fig. 25 *Prediction of the mean liquid temperature against the validation database.*

In Table 10, the indicators in Eqn. (**5**) are computed.

	Mean
$\|\varepsilon_T\|_{UPTF}$	10 °C
$\|\varepsilon_T\|_{TOPFLOW-PTS}$	2 °C

Table 10 *Absolute errors on the temperature with respect to the validation database.*

The discrepancies have the same order of magnitude with respect to the results in Table 9, showing a good capability of the model to predict the jet condensation when applied to the validation database and, in particular, to the UPTF tests (not used to develop the new correlation).

Thus, the model can be considered validated.

5. Conclusions

Three experiments with different geometrical configurations, namely COSI, TOPFLOW-PTS and UPTF, are studied to better understand the condensation phenomena occurring during the injection of a sub-cooled water jet in a circular pipe with a two-phase stratified flow.

After a thermal-hydraulic analysis, a total number of 110 tests are retained for the assessment of a new jet condensation model and 18 tests for its validation. The experimental conditions range between 0.3 and 7 MPa for the pressure, 0.06-161 kg/s for the injection flowrate and between 20 and 220 °C for the injection temperature. During the analysis of the experiments, it was found that a stratification can occur in the injection pipe which can have a strong impact on the calculation of the jet condensation. Thus, this study is limited to fully filled injection pipes.

New methodologies to average the mean liquid temperature of a thermocouple rake and for the estimation of the jet condensation mass flowrate were developed. The former identifies the last thermocouple in the liquid and averages the temperatures under the hypothesis of a uniform velocity field. The latter is based on the calculation of local heat balances between different thermocouple rakes and allows to determine the distribution of the condensation in the different zones of the test sections. It is then proven that most of the condensation occurs in the jet region, as usually assumed in the literature. The estimation of the heat exchange area is improved with respect to the other models found in the literature.

The correlations found in the literature modelled the condensation heat transfer coefficient through the Nusselt number. They were tested against the new revised assessment database, showing poor results. Thus, a new jet condensation model was developed with a different approach.

The jet is modelled as a heat exchanger and the condensation potential is defined. Its equation is analytically derived. It is shown that the condensation potential should follow an exponential function of a parameter η and of the shape factor L/d_{inj}, which is proportional to the ratio between the heat exchange and jet cross section areas.

A correlation for η is assessed as function of a steam potential Nusselt, an injection Reynolds and a Prandtl number. The steam potential Nusselt number takes into account the effect of the steam flowrate on the condensation.

The newly developed correlation shows good results. The mean liquid temperature is predicted with a mean error of 10 °C on the assessment database. Good predictions are also obtained on the 18 validation tests not used for the development of the model.

Acknowledgements

The current research project was conducted within a cooperation agreement between CEA (Commisariat à l'Energie Atomique et aux Energies Alternatives), EDF (Electricité de France), and Framatome. The authors gratefully acknowledge their financial support.

References

[1] N. Aksan, F. D'Auria, H. Glaeser, Thermal-hydraulic phenomena for water cooled nuclear reactors, Nuclear Engineering and Design 330 (2018) 166-186.

[2] Y. Finkelstein, A. Tamir, Interfacial Heat Transfer Coefficients of Various Vapors in Direct Contact Condensation, The Chemical Engineering Journal 12 (1976) 199-209.

[3] J.F. Maćkowiak, A. Górak, E.Y. Kenig, Modelling of combined direct-contact condensation and reactive absorption in packed columns, Chemical Engineering Journal 146 (2009) 362-369.

[4] I. Aya, H. Nariai, Evaluation of heat-transfer coefficient at direct-contact condensation of cold water and steam, Nuclear Engineering and Design 131 (1991) 17-24.

[5] S.R. Yang, J. Seo, Y.-A. Hassan, Thermal hydraulic characteristics of unstable bubbling of direct contact condensation of steam in subcooled water, International Journal of Heat and Mass Transfer 138 (2019) 580-596.

[6] Q. Zu, L. Guo, S. Zou, J. Chen, X. Zhang, Experimental study on direct contact condensation of stable steam jet in water flow in a vertical pipe, International Journal of Heat and Mass Transfer 66 (2013) 808-817.

[7] G. Gregu, M. Takahashi, M. Pellegrini, R. Mereu, Experimental study on steam chugging phenomenon in a vertical sparger, International Journal of Multiphase Flow 88 (2017) 87-98.

[8] C.-H. Song, S. Cho, H.-S. Kang, Steam Jet Condensation in a Pool: From Fundamental Understanding to Engineering Scale Analysis, Journal of Heat Transfer 134 (2012) 401-415.

[9] G.P. Celata, M. Cumo, G.E. Farello, G. Focardi, A comprehensive analysis of direct contact condensation of saturated steam on subcooled liquid jets, International Journal of Heat and Mass Transfer 32 (1989) 639-654.

[10] T. Seidel, M. Beyer, D. Lucas, U. Hampel, Experimental studies on high-pressure high-temperature contact-condensation at falling jets in the TOPFLOW pressure-tank, Nuclear Engineering and Design 336 (2018) 54-63.

[11] M. Takahashi, A.K. Nayak, S-.I. Kitagawa, H. Murakoso, Heat Transfer in Direct Contact Condensation of Steam to Subcooled Water Spray, Journal of Heat Transfer 123 (2001) 703-710.

[12] J. Liao, C. Frepoli, K. Ohkawa, Cold leg condensation model for analysing loss-of-coolant accident in PWR, Nuclear Engineering and Design 285 (2015) 171-187.

[13] A. Petrovic de With, R.K. Calay, G. de With, Three-dimensional condensation regime diagram for direct contact condensation of steam injected into water, International Journal of Heat and Mass Transfer 50 (2007) 1762-1770.

[14] V.S. Naik-Nimbalkar, A.W. Patwardhan, I. Banerjee, G. Padmakumar, G. Vaidyanathan, Thermal mixing in T-junctions, Chemical Engineering Science 65 (2010) 5901-5911.

[15] E.D. Hughes, R.B. Duffey, Direct Contact Condensation and Momentum Transfer in Turbulent Separated Flows, International Journal of Multiphase Flow 17 (1991) 599-619.

[16] D. Bestion, L. Gros d'Aillon, Condensation tests analysis and correlation for the CATHARE code, in: Proceedings of the Fourth International Topical Meeting on Nuclear Reactor Thermal-Hydraulics (NURETH-4), Braun, Karlsruhe, 1989.

[17] A. Janicot, D. Bestion, Condensation modelling for ECC injection, Nuclear Engineering and Design 145 (1993) 37-45.

[18] P. Weiss, UPTF experiments: Principal full-scale test results for enhanced knowledge of large break LOCA scenarios in PWR's, in: Proceedings of the Fourth international topical meeting on nuclear reactor thermal-hydraulics (NURETH-4), Braun, Karlsruhe, 1989.

[19] W.-Y. Ren, G.-J. Yu, J.-W. Bian, W.-X. Tian, G.-H. Su, S.-Z. Qiu, X.-L. Fu, Experiment of Condensation in T-junction: Steam-water Flow in Water-injected Condition, in: Proceedings of the 16th international topical meeting on nuclear reactor thermal-hydraulics (NURETH-16), Chicago, USA, 2015.

[20] P. Gaillard, M.-G. Rodio, A general thermal stratification criterion for single and two-phase flows in a pipe after subcooled injection, International Journal of Multiphase Flow 101 (2018) 1-10.

[21] P. Péturaud, U. Hampel, A. Barbier, J. Dreier, F. Dubois, E. Hervieu, A. Martin, H.-M. Prasser, General overview of the TOPFLOW-PTS experimental program, in: Proceedings of the 14th international topical meeting on nuclear reactor thermal-hydraulics (NURETH-14), Toronto, Canada, 2011.

[22] H.-M. Prasser, U. Hampel, P. Schütz, TOPFLOW pressure chamber – Versatile techniques to simplify design and instrumentation of therml fluid dynamic experiments at high pressure, Nuclear Engineering and Design 372 (2021) 110971.

[23] B.H. Thacker, S.W. Doebling, F.M. Hemez, M.C. Anderson, J.E. Pepin, E.A. Rodriguez, Concepts of model verification and validation, LA-14167-MS, Los Alamos National Laboratory, 2004.

[24] D. Lucas, M. Beyer, and E. Krepper, TOPFLOW-experiments, development and validation of CFD models for steam-water flows with phase transfer. Final report, No. HZDR—011, Helmholtz-Zentrum Dresden-Rossendorf eV, 2011.

[25] P. Coste, N. Mérigoux, Two-phase CFD validation: TOPFLOW-PTS steady-state steam-water tests 3-16, 3-17, 3-18 and 3-19, Nuclear Engineering and Design 299 (2016) 18-27.

[26] T. Seidel, M. Beyer, U. Hampel, D. Lucas, TOPFLOW-PTS air-water experiments on the stratification in the ECC nozzle and the ECC water mixing during PTS scenarios, in: Proceedings of the 14th international topical meeting on nuclear reactor thermal-hydraulics (NURETH-14), Toronto, Canada, 2011.

[27] Siemens AG, Division Production d'Energie, Essai C1/C2 Refroidissement par panache et par lame de la paroi de la cuve, NT31/96/17 (1996).

[28] H. Press, R. Schröder, Hydrodynamik im Wasserbau (Hydrodynamic in hydraulic structures), Ernst & Sohn, Berlin, 1966.

[29] R. Cocci, G. Damblin, A. Ghione, L. Sargentini, D. Lucor, A comprehensive Bayesian framework for the development, validation and uncertainty quantification of thermalhydraulic models, Annals of Nuclear Energy 172 (2022) 109029.

[30] T.O. Kvålseth, Note on the R2 measure of goodness of fit for nonlinear models, Bulletin of the Psychonomic Society 21 (1983) 79-80.

[31] J. Iciek, The hydrodynamics of a free, liquid jet and their influence on direct contact heat transfer—III. Direct contact heating of a cylindrical, free falling liquid jet, International Journal of Multiphase Flow 9 (1983) 167-179.

[32] B. Clausnitzer, W.H. Hager, Outflow Characteristics from Circular Pipe, Journal of Hydraulic Engineering 123 (1997) 914-917.

[33] R.H. Whittle, R. Forgan, A correlation for the Minima in Pressure Drop Versus Flow-rate Curves for Sub-cooled Water Flowing in Narrow Heated Channels, Nuclear Engineering and Design 6 (1967) 88-89.

[34] R. Stelling, E.V. McAssey Jr., T. Dougherty, B.W. Yang, The Onset of Flow Instability for Downward Flow in Vertical Channels, Journal of Heat Transfer 118 - Transactions of the ASME (1996) 709-714.

[35] F. X. Buschman, D. Aumiller, Use of fundamental condensation heat transfer experiments for the development of a sub-grid liquid jet condensation model, Nuclear Engineering and Design 312 (2017) 147-160.

[36] I.S. Lim, R.S. Tankin, M.C. Yuen, Condensation Measurement of Horizontal Cocurrent Steam/Water Flow, Journal of Heat Transfer 106 - Transactions of the ASME (1984) 425-432.

[37] H.J. Kim, S.C. Lee, S.G. Bankoff, Heat transfer and interfacial drag in countercurrent steam-water stratified flow, International Journal of Multiphase Flow 11 (1985) 593-606.